

Phase Diagram of an Extended Quantum Dimer Model on the Hexagonal Lattice

Thiago Schlittler,^{1,*} Thomas Barthel,^{2,3,†} Grégoire Misguich,^{4,‡} Julien Vidal,^{1,§} and Rémy Mosseri^{1,||}
¹Laboratoire de Physique Théorique de la Matière Condensée, CNRS UMR 7600, Université Pierre et Marie Curie,
 Sorbonne Universités, 4 Place Jussieu, 75252 Paris Cedex 05, France

²Laboratoire de Physique Théorique et Modèles Statistiques, Université Paris-Sud,
 CNRS UMR 8626, 91405 Orsay Cedex, France

³Department of Physics, Duke University, Durham, North Carolina 27708, USA

⁴Institut de Physique Théorique, Université Paris Saclay, CEA, CNRS, F-91191 Gif-sur-Yvette, France

(Received 16 July 2015; published 18 November 2015)

We introduce a quantum dimer model on the hexagonal lattice that, in addition to the standard three-dimer kinetic and potential terms, includes a competing potential part counting dimer-free hexagons. The zero-temperature phase diagram is studied by means of quantum Monte Carlo simulations, supplemented by variational arguments. It reveals some new crystalline phases and a cascade of transitions with rapidly changing flux (tilt in the height language). We analyze perturbatively the vicinity of the Rokhsar-Kivelson point, showing that this model has the microscopic ingredients needed for the “devil’s staircase” scenario [Eduardo Fradkin *et al.* Phys. Rev. B 69, 224415 (2004)], and is therefore expected to produce fractal variations of the ground-state flux.

DOI: 10.1103/PhysRevLett.115.217202

PACS numbers: 75.10.Jm, 05.30.Rt, 05.50.+q

The study of hard-core dimer coverings has a long history. From the mapping to Pfaffians and determinants by Kasteleyn [1,2], the solution of two-dimensional Ising models [3], the height representation and its continuum limit [4], or the connection to the Coulomb gas and conformal field theory [5,6], dimer models have found numerous applications in various fields of statistical physics. Motivated by the physics of resonating valence bond systems, Rokhsar and Kivelson (RK) [7] added quantum dynamics to the dimer model, leading to the so-called quantum dimer model (QDM), which later led to tractable models with rich phase diagrams closely related to lattice gauge theories [8]. Importantly, QDMs appeared in different contexts when describing the dynamics in a constrained low-energy manifold, such as in frustrated Ising models in weak transverse fields [9]. QDMs also gained a new dimension with the discovery of liquid phases with topological order in nonbipartite lattices [10,11], where they shed some light on the long-sought resonating valence bond liquids. This field also benefited from recent progress in making quantitative connections between spin-1/2 Heisenberg magnets with quantum disordered ground states and QDMs [12,13].

In most QDMs studied so far, a kinetic term (associated with on-plaquette dimer flips) competes with a diagonal term proportional to the number of such “flippable” plaquettes. When the kinetic and the potential terms are equal at the so-called RK point, the ground states are exactly known [7]. In the height language, appropriate for bipartite lattices, such a RK point corresponds to a transition from a “flat” phase to a maximal slope phase [14]. A richer behavior is however expected near that point for more generic interactions between dimers [16,17]. In

particular, within a field theoretic approach, a devil’s staircase of commensurate and incommensurate phases is predicted [16–18], corresponding to a fractal tilt variation as a function of the Hamiltonian parameters.

In this Letter, we show that a natural generalization of the hexagonal lattice QDM [19,20] provides a microscopic model with this phase structure. We analyze the two-parameter phase diagram spanned by the standard potential term counting flippable plaquettes and another term counting dimer-free plaquettes. The model is studied perturbatively near the RK point and with quantum Monte Carlo (QMC) simulations elsewhere, supplemented by variational arguments. We observe a sequence of closely spaced phase transitions with a gradual change of the flux density and crystalline structures with strongly varying unit cell sizes in agreement with the scenario of Refs. [16,17].

Model.—Let us consider a QDM with the standard kinetic term and four potential terms:

$$\hat{H} = -t \sum_h (|\uparrow\downarrow\rangle\langle\downarrow\uparrow| + \text{h.c.}) + \sum_{j=0}^3 v_j \hat{n}_j, \quad (1)$$

where the operator \hat{n}_j counts the total number of hexagonal plaquettes with j dimers (called a j -plaquette). Because of the two sum rules [20,21] $\hat{n}_0 + \hat{n}_1 + \hat{n}_2 + \hat{n}_3 = N$ and $2\hat{n}_0 + \hat{n}_1 - \hat{n}_3 = 0$, these potential terms are not independent and we hence choose to keep only \hat{n}_0 and \hat{n}_3 . Also, we denote densities $\rho_j = \langle \hat{n}_j \rangle / N$ in the form $\vec{\rho} = (\rho_0, \rho_1, \rho_2, \rho_3)$ and fix $t = 1$, unless specified differently. The model studied by Moessner *et al.* [19] has $v_0 = 0$, while the two models ($v_0 = \pm 1, v_3 = 0$) are relevant for Ising string nets [28]. We study rectangular

clusters with periodic boundary conditions and $N = L_x \times L_y$ hexagonal plaquettes.

Our analysis relies on the notion of flux: dimer coverings can be grouped into topological sectors [21] labeled by two integer fluxes (F_x, F_y) , which are invariant under local dimer moves. As discussed below, for ground states, one of the two fluxes is zero and we can restrict ourselves to $F_x = 0$ and work with $f := F_y/L_y \geq 0$.

Classical limit.—Let us consider the classical limit $t = 0$. Setting $v_0 = \sin \alpha$, $v_3 = \cos \alpha$, and defining $\alpha_1 = \arctan(-2)$, $\alpha_2 = \pi/2 - \alpha_1$, one finds three crystals as α is varied: (i) for $\alpha \in [\pi/2, \alpha_1]$, the threefold degenerate staggered crystals (nonflippable configurations) with maximum flux $f = 2$, vanishing energy, and $\vec{\rho} = (0, 0, 1, 0)$, (ii) for $\alpha \in [\alpha_1, \alpha_2]$, the (threefold degenerate) star crystal in the $f = 0$ sector (Fig. 1) with $\vec{\rho} = (1/3, 0, 0, 2/3)$, (iii) for $\alpha \in [\alpha_2, \pi/2]$, a 12-fold degenerate crystal [29] denoted S_2 , within the $f = 1/2$ sector, with $\vec{\rho} = (0, 1/2, 0, 1/2)$. The point $\alpha = \pi/2$ is highly degenerate, since any configuration without 0-plaquettes is a ground state, and such states exist in all flux sectors. This degeneracy is lifted when $t \neq 0$, leading to a nontrivial ground-state flux variation as discussed below.

Phase diagram.—We studied the phase diagram with QMC simulations using the mapping to an Ising-type

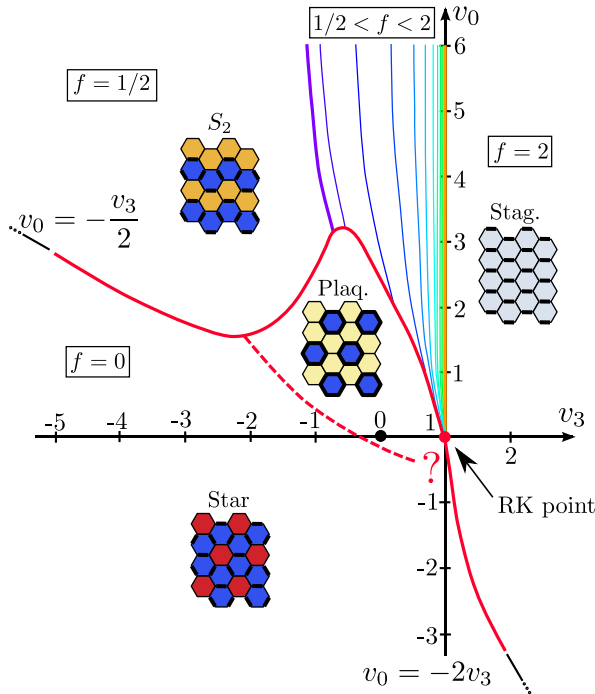


FIG. 1 (color online). Schematic phase diagram from QMC simulations ($L_x = L_y = 60$). The (v_0, v_3) plane is divided into five regions: a staggered phase with the maximal flux ($f = 2$), the star and the plaquette phases ($f = 0$), the S_2 phase ($f = 1/2$), and the fan region, containing a cascade of flux sectors $1/2 \leq f < 2$. The plaquette color indicates the dimer density (same scale as in Figs. 2 and 3).

model described in Refs. [19–21]. Specifically, results displayed in Fig. 1 have been obtained for a torus with 60×60 plaquettes, flux sectors $f = 0, \frac{1}{10}, \frac{2}{10}, \dots, 2$, inverse temperature $\beta = 9.6$, and imaginary-time step $\Delta\beta = 0.01$.

(1) $f = 2$. In this region, ground states are isolated staggered configurations with vanishing energy. The Hamiltonian is positive definite in the upper right quadrant, and the $f = 2$ region also extends to a large part of the lower right quadrant, down to the boundary with the $f = 0$ sector.

(2) $f = 0$. The star and plaquette crystals found in this region also exist in the v_3 -only model [19,20] and are separated by a first-order transition (dashed line). The star phase is adiabatically connected to the (threefold degenerate) crystalline configurations found for $t = 0$. The latter simultaneously maximize the number of 3- and 0-plaquettes, and the star phase thus fills a large part of the $(v_3 < 0, v_0 < 0)$ -quadrant and also extends into the neighboring quadrants. On the $v_0 = 0$ line, the star phase gives way to the plaquette phase through a first-order transition at $v_3 = -0.228(2)$ [19,20]. The plaquette phase is defined by continuity with the “ideal” plaquette state, which is an uncorrelated product of resonating 3-plaquettes $|\uparrow\downarrow\uparrow\rangle + |\downarrow\uparrow\downarrow\rangle$. In the vicinity of the RK point, as is already the case for $\hat{H}(t, v_0 = 0, v_3)$ [20], the large (diverging) correlation length makes it difficult to discriminate numerically between the star and plaquette phases, hence the question mark in Fig. 1. This phenomenon is likely to be related to the $U(1)$ regime observed in the square lattice QDM [15].

(3) $f = 1/2$. In most of this region, the system forms a 12-fold degenerate crystalline phase, adiabatically connected to the S_2 configuration.

(4) $1/2 < f < 2$. This is the most interesting part of the phase diagram, which we call the fan region. To understand the flux variations taking place there, we recall that any dimer configuration can be represented equivalently as a configuration of nonintersecting strings on the hexagonal lattice [21]. For $F_x = 0$, these are $N_s = (2L_y - F_y)/3$ closed loops along the toroidal x direction of the lattice. Starting from the staggered dimer covering ($f = 2$) displayed in Fig. 1, on each string path, empty and covered edges alternate. The corresponding dimer covering is obtained by doing so-called loop updates, i.e., exchanging empty and covered edges along the string paths. Each string reduces the flux F_y by 3 units. In reverse, starting from an arbitrary configuration, the strings correspond to paths where dimer-free horizontal edges alternate with dimers on tilted edges (see Fig. 2). The number of 3-plaquettes along a string is maximized if it runs parallel to one of the three edge orientations of the lattice. This is why, for $v_3 < 1$, strings are on average parallel to one of the edge orientations and why ground states are found in sectors with one vanishing flux quantum number (F_x vanishes for strings winding in the x direction only). Strings can reduce

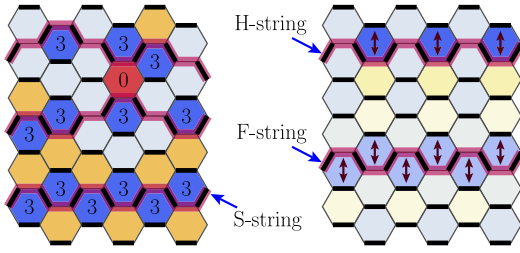


FIG. 2 (color online). Left: a configuration of three strings and the corresponding dimer covering, with 0- and 3-plaquettes. Left bottom and right: three variational classes of dynamically constrained strings, called *S*, *H*, and *F* strings. *S* strings are in a static zigzag configuration, *H* strings (*F* strings) are allowed to fluctuate by one row in every second column (in every column). Arrows indicate the fluctuations of the strings, each corresponding to a 3-plaquette flip. Dimer densities are indicated according to the color scale of Fig. 3. For *H* and *F* strings, the shown dimer densities correspond to a superposition of the allowed configurations.

their kinetic energy by oscillating in the perpendicular direction, limited by the string noncrossing condition and by avoidance of 0-plaquettes for large v_0 (see Fig. 2).

When v_3 is decreased below 1, the staggered configuration is destabilized by string insertion. At low string densities (f slightly below 2) strings are far apart and strongly delocalized. A reduction of v_3 causes an increase of ρ_3 , which is realized through a higher string density (decrease of the flux) and “stiffer” strings (reduced lateral motion). Each time a new string is added upon decreasing v_3 , the increased ρ_3 compensates the energy cost associated with the higher degree of localization. When increasing v_0 for a fixed $v_3 < 1$, configurations with more 0-plaquettes become less favorable such that string delocalization gets more restricted. At certain transition points, it becomes favorable to remove a string (flux increase), freeing some space for other strings to fluctuate more freely. When ρ_0 becomes negligible, a further increase of v_0 has no effect. This regime, where the isoflux lines become parallel, is equivalent to perturbing the (degenerate) classical point $(t, v_0, v_3) = (0, 1, 0)$ with a weak t and v_3 , where a “fan”-like phase diagram similar to that described in Ref. [30] is expected.

For $f \lesssim 1$ the average interstring distance is sufficiently low that the ground states are dominated by straight-string configurations. For generic fluxes, one expects complex correlated string states (some are described in Ref. [21]), but simple spatial structures involving horizontal chains of hexagons with higher densities of 3-plaquettes are also observed in some low-flux parts of the fan (see Fig. 3). These can be qualitatively understood in terms of the following typical configurations of strings that are dynamically constrained by the presence of neighboring strings: “*S* strings” are static zigzag configurations (corresponding to zigzag arrangements of 3-plaquettes, energetically favored at large negative v_3). With respect to such a reference

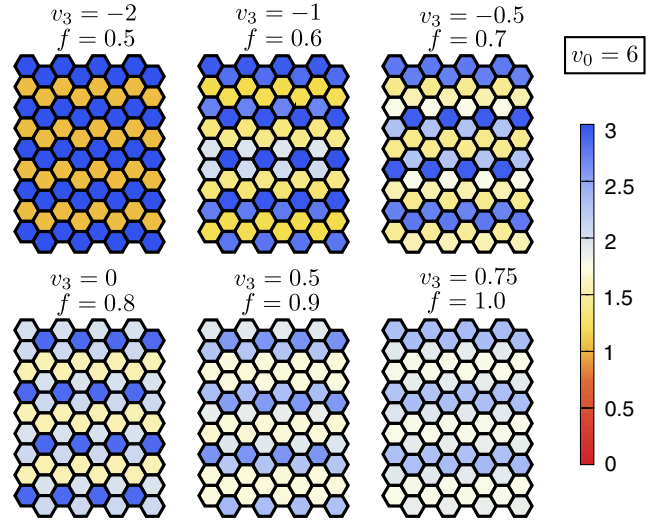


FIG. 3 (color online). Dimer density per hexagon in the fan region, according to the color scale on the right.

configuration, “*H* strings” can fluctuate in every second column of hexagons, up and down by one row. “*F* strings” are the most mobile among the three classes, and are allowed to fluctuate up and down by one row in every column as indicated by arrows in Fig. 2. At $f = 0.8$ and 1, for instance, we recognize periodic arrays of *H* (*F*) strings at distance $d = 2.5$ ($d = 3$) [31], as shown in Fig. 3. Importantly, no 0-plaquettes are generated if the above strings have minimum interstring distances of $d_{S-S}^{\min} = 2$, $d_{H-H}^{\min} = 2.5$, $d_{F-F}^{\min} = 3$, and $d_{F-H}^{\min} = 2.75$. These building blocks are therefore appropriate to describe qualitatively the large- v_0 and $f \lesssim 1$ part of the fan [21].

Finally, simple variational arguments provide approximate expressions for the flux transition lines. For example, one can compute the energy change associated with the insertion of an *H* string in a perfect S_2 crystal (*S* strings at distance 2), which corresponds to an infinitesimal increase of the flux density (due to the different d^{\min} , five *S* strings should be replaced by four *H* strings to keep the total system size constant [21]). This yields $v_3 = -1$ for the transition towards the fan region at large v_0 , in reasonable agreement with the numerics.

As the interplay between v_3 and v_0 is especially complex for low v_0 (when ρ_0 is not negligible), we analyzed the $v_3 = 0$ line with finer flux steps. Starting from very large v_0 the flux decreases (staying close to $f = 0.8$) down to $v_0 \approx 2.4$ where it drops to $f = 0$. This flux drop is a generic feature of the interface with the $f = 0$ region. Toward the RK point the ground-state flux sectors get pinched, a feature that we now discuss.

Perturbative analysis.—At the RK point, the ground states of all flux sectors are degenerate, and are equal-amplitude superpositions of all dimer configurations in the corresponding sector. At first order in v_0/t and $(v_3 - 1)/t$, the energy density in sector f reads $e(f) = v_0\rho_0(f) + (v_3 - 1)\rho_3(f)$.

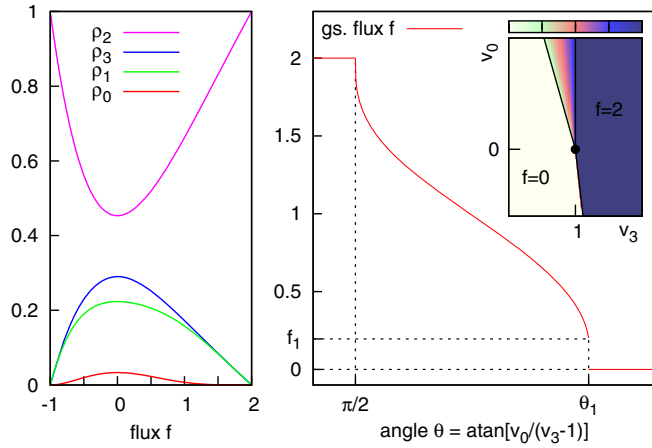


FIG. 4 (color online). Perturbation theory near the RK point. Left: j -plaquette densities ρ_j as functions of the flux density f . Right: ground-state flux density f as a function of the angle θ that parametrizes the perturbation. The nontrivial region lies between $\pi/2$ (transition out of the staggered phase) and $\theta_1 \approx 1.84695$, where f drops discontinuously from $f_1 \approx 0.195654$ to 0. The transition from $f = 0$ to $f = 2$ occurs at $\theta_2 \approx 4.8268$ (not shown).

We compute the j -plaquette densities $\rho_j(f)$ as expectation values of the operators \hat{n}_j (diagonal in the dimer basis) with respect to the unperturbed RK states, using an analytical transfer-matrix approach [21,32]. Setting $v_0 = \sin \theta$ and $v_3 - 1 = \cos \theta$, we minimize $e(f)$ for each value of θ to obtain $f(\theta)$ as displayed in Fig. 4. A continuous variation of f is found in the interval $\theta \in [\pi/2, \theta_1 \approx 1.84695]$, which corresponds to the fan region in the phase diagram of Fig. 1. Interestingly, f jumps discontinuously to zero at θ_1 . For $\theta \in [\theta_1, \theta_2 \approx 4.8268]$, the ground state is in the $f = 0$ flux sector, and it jumps to $f = 2$ for $\theta \in [\theta_2, \pi/2]$. Note that, at this order, wave functions remain RK states, which are translation-invariant dimer liquids with algebraic correlations (for $f < 2$).

Field theory.—To connect our perturbative and numerical results concerning the flux variations, let us turn to the height representation [4,18,33–35]. Dimer coverings are mapped to membranes embedded in a cubic lattice, whose average tilt is directly related to the flux [36]. In this language the QDM becomes a quantum roughening problem [18]. Long-distance properties are captured by taking the continuum limit of the height model and, in our case, the RK point is described by a massless Gaussian field theory [35]. Fradkin *et al.* [16] and Vishwanath *et al.* [17] discussed how the action is modified in the presence of generic perturbations, through a renormalization group (RG) analysis [37] predicting nonvanishing flux phases. A cubic interaction for the height, with three spatial derivatives, is the leading term favoring $f \neq 0$. In our problem we observe that v_0 induces a flux density perpendicular to some edges of the hexagonal lattice. This implies that the sign of the corresponding coupling

is negative in the notation of Ref. [16]. At this stage, the system would be gapless with a linear dispersion at small momenta. However, the site positions and the microscopic heights are both discrete and form a 3D lattice \mathcal{L} . For the (coarse-grained) height field, potential terms that respect the symmetries of \mathcal{L} will be generated upon integration over the short-distance fluctuations. They can be written as $V(h, \vec{r}) = \sum_{\mathbf{K}=(K_0, \vec{K}) \in \mathcal{L}^*} V_{\mathbf{K}} e^{i(K_0 h + \vec{K} \cdot \vec{r})}$, where the sum runs over the reciprocal lattice vectors of \mathcal{L} . When the average flux (tilt) is commensurate with the lattice, it corresponds to some reciprocal lattice vector \mathbf{K} and the associated locking term $V_{\mathbf{K}}$ is then asymptotically relevant in the RG [16], leading to gapped crystals. However, as explained in Ref. [16], these gaps can become exponentially small in $1/f$ close to the RK point. Since crystals for rational fluxes with small denominators are more stable, their range of attraction in the RG is larger compared to others and, for the phase diagram close to the RK point, one thus expects a fractal succession of commensurate phases—a “devil’s staircase.” At the smaller fluxes, stronger quantum fluctuations can outweigh locking terms and impose irrational flux densities such that gapless incommensurate structures are possible.

Conclusion.—The extended QDM (1) is the first candidate for a microscopic realization of the “Cantor deconfinement” scenario, which predicts that a fractal succession of flux sectors occurs near the RK point. Whether the flux varies continuously, in a fractal way, or assumes only a finite number of values [38] is impossible to answer with QMC simulations. Indeed, although we can simulate large lattices, available flux sectors correspond to a small set of rational values. Additionally, intrasector gaps become very small near the RK point and render simulations difficult. However, the fact that all flux sectors for $1/2 < f < 2$ occur in the QMC results and the width variations of the corresponding regions in the phase diagram plead in favor of the realization of a fractal in the thermodynamic limit.

Finally, let us note that flux sequences found here cannot occur for square lattice models with single-plaquette Hamiltonians. In that case, the sum rule $n_0 = n_2$ makes any QDM with potential terms $\sum_j v_j \hat{n}_j$ equivalent to the original RK model, which lacks intermediate-flux phases.

We wish to thank S. Capponi for useful discussions. G. M. is supported by a JCJC grant from the Agence Nationale pour la Recherche (Project No. ANR-12-JS04-0010-01).

* thiago.schlittler@upmc.fr

† <http://www.manyparticle.org/~barthel/>

‡ gregoire.misguich@cea.fr

§ vidal@lptmc.jussieu.fr

|| remy.mosseri@upmc.fr

[1] P. Kasteleyn, *Physica (Utrecht)* **27**, 1209 (1961).

[2] M. E. Fisher, *Phys. Rev.* **124**, 1664 (1961).

- [3] M. E. Fisher, *J. Math. Phys. (N.Y.)* **7**, 1776 (1966).
- [4] H. W. J. Blöte and H. J. Hilhorst, *J. Phys. A* **15**, L631 (1982).
- [5] F. Alet, J. L. Jacobsen, G. Misguich, V. Pasquier, F. Mila, and M. Troyer, *Phys. Rev. Lett.* **94**, 235702 (2005).
- [6] S. Papanikolaou, E. Luijten, and E. Fradkin, *Phys. Rev. B* **76**, 134514 (2007).
- [7] D. S. Rokhsar and S. A. Kivelson, *Phys. Rev. Lett.* **61**, 2376 (1988).
- [8] E. Fradkin and S. Kivelson, *Mod. Phys. Lett. B* **04**, 225 (1990).
- [9] R. Moessner and S. L. Sondhi, *Phys. Rev. B* **63**, 224401 (2001).
- [10] R. Moessner and S. L. Sondhi, *Phys. Rev. Lett.* **86**, 1881 (2001).
- [11] G. Misguich, D. Serban, and V. Pasquier, *Phys. Rev. Lett.* **89**, 137202 (2002).
- [12] D. Poilblanc, M. Mambrini, and D. Schwandt, *Phys. Rev. B* **81**, 180402 (2010).
- [13] I. Rousochatzakis, Y. Wan, O. Tchernyshyov, and F. Mila, *Phys. Rev. B* **90**, 100406 (2014).
- [14] See Ref. [15] and references therein for the latest numerical results on the square lattice QDM phase diagram.
- [15] D. Banerjee, M. Bögli, C. P. Hofmann, F.-J. Jiang, P. Widmer, and U.-J. Wiese, *Phys. Rev. B* **90**, 245143 (2014).
- [16] E. Fradkin, D. A. Huse, R. Moessner, V. Oganesyan, and S. L. Sondhi, *Phys. Rev. B* **69**, 224415 (2004).
- [17] A. Vishwanath, L. Balents, and T. Senthil, *Phys. Rev. B* **69**, 224416 (2004).
- [18] L. S. Levitov, *Phys. Rev. Lett.* **64**, 92 (1990).
- [19] R. Moessner, S. L. Sondhi, and P. Chandra, *Phys. Rev. B* **64**, 144416 (2001).
- [20] T. M. Schlittler, R. Mosseri, and T. Barthel, arXiv:1501.02242.
- [21] See Supplemental Material at <http://link.aps.org/supplemental/10.1103/PhysRevLett.115.217202>, which includes Refs. [22–27], for some details about the flux sectors, the string and the height representations, the dimer sum rules, the classical limit, the QMC method, the perturbation theory around the RK point, and certain variational states.
- [22] P. Orland, *Phys. Rev. B* **47**, 11280 (1993).
- [23] R. Moessner and K. S. Raman, arXiv:0809.3051.
- [24] J.-F. Sadoc and R. Mosseri, *Geometrical Frustration* (Cambridge University Press, Cambridge, England, 1999).
- [25] M. Suzuki, S. Miyashita, and A. Kuroda, *Prog. Theor. Phys.* **58**, 1377 (1977).
- [26] J. Propp, arXiv:math/0209005.
- [27] A. Feiguin, S. Trebst, A. W. W. Ludwig, M. Troyer, A. Kitaev, Z. Wang, and M. H. Freedman, *Phys. Rev. Lett.* **98**, 160409 (2007).
- [28] M. D. Schulz, S. Dusuel, G. Misguich, K. P. Schmidt, and J. Vidal, *Phys. Rev. B* **89**, 201103 (2014).
- [29] The factor 12 is due to three equivalent orientations for the chains of 3-plaquettes, two translations perpendicular to the chains, and the period of 2 along the chains.
- [30] S. Papanikolaou, K. S. Raman, and E. Fradkin, *Phys. Rev. B* **75**, 094406 (2007).
- [31] String distances d are measured in units of the distance between hexagon centers.
- [32] J.-M. Stéphan, S. Furukawa, G. Misguich, and V. Pasquier, *Phys. Rev. B* **80**, 184421 (2009).
- [33] R. Youngblood, J. D. Axe, and B. M. McCoy, *Phys. Rev. B* **21**, 5212 (1980).
- [34] B. Nienhuis, H. J. Hilhorst, and H. W. J. Blöte, *J. Phys. A* **17**, 3559 (1984).
- [35] C. L. Henley, *J. Stat. Phys.* **89**, 483 (1997).
- [36] A vanishing flux corresponds to membranes being, on average, normal to the (1,1,1) direction.
- [37] G. Grinstein, *Phys. Rev. B* **23**, 4615 (1981).
- [38] Note that at sudden jumps of the flux from f' to $f'' > f'$, as occurs in the numerical and perturbative phase diagrams of Figs. 1 and 4, all fluxes in $[f', f'']$ are degenerate. In doubt, the corresponding ground states can always be realized as phase-separated states of fluxes f' and f'' .